High-frequency internal waves and thick bottom mixed layers observed by gliders in the Gulf Stream

Robert E. Todd[1]

Corresponding author: R. E. Todd, Physical Oceanography Department, Woods Hole Oceanographic Institution, 266 Woods Hole Rd. MS #21, Woods Hole, MA 02543, USA. (rtodd@whoi.edu)

[1]Department of Physical Oceanography,
Woods Hole Oceanographic Institution,
Woods Hole, MA, USA.

Key Points.

- Spray gliders provide high-resolution surveys of the Gulf Stream along the U.S. East Coast.
- High-frequency internal lee waves are generated by Gulf Stream flow over Blake Plateau.
- Thick bottom mixed layers are common over Blake Plateau.

Autonomous underwater gliders are conducting high-resolutions surveys within the Gulf Stream along the U.S. East Coast. Glider surveys reveal two mechanisms by which energy is extracted from the Gulf Stream as it flows over the Blake Plateau, a portion of the outer continental shelf between Florida and North Carolina where bottom depths are less than 1000 m. Internal waves with vertical velocities exceeding 0.1 m s^{-1} and frequencies just below the local buoyancy frequency are routinely found over the Blake Plateau, particularly near the Charleston Bump, a prominent topographic feature. These waves are likely internal lee waves generated by the sub-inertial

Gulf Stream flow over the irregular bathymetry of the outer continental shelf. Bottom mixed layers with O(100) m thickness are also frequently encountered; these thick bottom mixed layers likely form in the lee of topography due to enhanced turbulence generated by O(1) m s^{-1} near-bottom flows.

1. Introduction

As a subtropical western boundary current, the Gulf Stream is a major reservoir of oceanic kinetic energy [e.g., *Wyrtki et al.*, 1976], which is input globally by winds and tides at rates of approximately 1 TW [*Wunsch*, 1998] and 3.5 TW [*Munk and Wunsch*, 1998], respectively. Understanding mechanisms by which the ocean's kinetic energy is ultimately lost through friction or dissipated through mixing (i.e., converted to potential energy) to maintain the observed abyssal stratification is a central theme in physical oceanography. Rather than mixing and dissipation being uniform over the world's oceans [e.g., *Munk*, 1966], a number of observational programs over the past decades have demonstrated that enhanced mixing occurs where strong flows encounter topographic features, generating internal waves that break locally or farther away and inducing turbulent mixing in the lee of topopgraphy. Thus far, these studies have focused primarily on tidal flows over ridges or sills [e.g., *Polzin et al.*, 1997; *Rudnick et al.*, 2003; *Klymak et al.*, 2006; *Martin and Rudnick*, 2007; *Cole et al.*, 2009; *Alford et al.*, 2011; *Rudnick et al.*, 2013], abyssal flows over topography [e.g., *Polzin et al.*, 1996; *Ferron et al.*, 1998], and the Antarctic Circumpolar Current as it encounters topography [e.g., *St. Laurent et al.*, 2012]; here we show that similar transfer of energy from the large-scale flow to internal waves and near-bottom mixing occurs as the Gulf Stream flows along the continental margin.

Before separating from the continental margin near Cape Hatteras, the Gulf Stream flows over the varied bathymetry of the Blake Plateau (Fig. 1a; *Pratt and Heezen* [1964]) where water depths are less than 1000 m and bottom velocities of approximately 0.25 m s^{-1} were first measured by *Pratt* [1963]. Near 31.5°N, 79°W, a ridge and trough feature in the continental slope, referred to as the Charleston Bump (Fig. 1b), is known to deflect the path of the Gulf Stream [e.g., *Brooks and Bane*, 1978]. Recent numerical simulations by *Gula et al.* [2015] have shown that the Charleston Bump steers the Gulf Stream through bottom pressure torque and plays a significant role in transfer of energy between eddies and the mean flow.

The response of flow to encountering topographic features depends on the size of the obstacle relative to the flow speed and stratification as characterized by the topographic Froude number, $F_{\text{topo}} \equiv U/NH$, where U is the near-bottom flow speed, N is the near-bottom stratification, and H is the height of the obstacle [*Bell*, 1975; *Gill*, 1982; *Klymak et al.*, 2010]. For topographic Froude numbers greater than unity, small-amplitude linear lee waves form [e.g., *Bell*, 1975]. As the topographic Froude number becomes smaller than unity, lee waves become nonlinear [e.g., *Miles and Huppert*, 1968, their Figs. A1–A4] and streamlines can become statically unstable in a stratified hydraulic jump downstream of the obstacle [*Klymak et al.*, 2010]. *Dossmann et al.* [2016] point out that significant radiation of lee waves only occurs when the lateral Froude number $F_L \equiv U/NL$ is less than O(1) for a horizontal topographic scale L; flow over the Blake Plateau and Charleston Bump generally satisfies this criterion. Both breaking of the internal waves and static instability lead to mixing and energy dissipation. *Dossmann et al.* [2016] examined the flow response over a range for topographic Froude numbers in laboratory experiments, finding that near-bottom mixing occurs for a wide range of topographic Froude numbers while resonance between the background flow and internal lee waves leads to radiation and remote mixing only for $F_{\text{topo}} \sim 1-2$. *Nikurashin and Ferrari* [2011] recently estimated that about 20% of the wind power input to the global ocean can be accounted for by energy conversion from geostrophic flows to internal lee waves in the deep ocean, but possible energy conversion over the relatively shallow Blake Plateau and Charleston Bump were not part of their analysis.

High-resolution surveys of the Gulf Stream from autonomous underwater gliders reveal that large-amplitude, high-frequency internal lee waves and thick bottom mixed layers commonly occur where the Gulf Stream flows over the outer continental shelf southwest of Cape Hatteras. The remainder of this paper is organized as follows: section 2 describes glider observations in the Gulf Stream, section 3.1 characterizes observed lee waves, section 3.2 discusses bottom mixed layers, and section 4 summarizes the results and implications.

2. Glider Observations in the Gulf Stream

Spray underwater gliders [*Sherman et al.*, 2001] first surveyed across the Gulf Stream downstream of Cape Hatteras from 2004 to 2009; those glider missions are described by *Todd et al.* [2016]. Since 2015, Spray gliders have been surveying the Gulf Stream between Miami, Florida and New England. These missions typically begin with deployment from a small boat a few miles offshore of Miami in the Florida Strait at approximately 25.75°N, 80.0°W, and recovery is intended to be over the continental shelf south of Woods Hole, Massachusetts. The current sampling goal is to collect measurements along approximately 10 transects across the Gulf Stream during each glider mission. Since the 0.25 m s^{-1} horizontal speed of a glider through the water is much less than the vertically averaged speed of the Gulf Stream, which can exceed 1 m s^{-1}, gliders are advected downstream as they cross the Gulf Stream, resulting in zigzag sampling patterns over the bottom (Fig. 1c). Gliders are often navigated upstream relative to the Gulf Stream in more quiescent waters on either side of the boundary current. In a coordinate system moving with the water, the cross-Gulf Stream glider transects are approximately orthogonal to the flow.

Here we use observations from ten Spray glider missions completed between 2004 and early 2017. We refer to the missions using a shorthand that includes the year and month of deployment and glider serial number as YYMSSS, where YY is the last two digits of the year, M is the month in hexadecimal, and SSS is the glider's serial number. Observations in this analysis are from missions 049007, 056007, 05C007, 08B021, 154010, 157055, 15A065, 15C066, 168066, and 16B056. Trajectories and summary statistics for these missions are shown in Fig. 1c.

Each glider was equipped with a pumped Sea-Bird 41CP conductivity-temperature-depth (CTD) instrument, and missions 157055, 15A065, 15C066, 168066, and 16B056 additionally carried Seapoint chlorophyll fluorometers plumbed in line with the CTDs and 1-MHz Nortek AD2CP Doppler current profilers. The gliders sampled the upper 1000 meters of the water column or to within several meters of the bottom in shallower water; to avoid hitting the seafloor, gliders with AD2CPs detected the bottom acoustically and maximum dive depths for gliders without AD2CPs were chosen based on bathymetric maps. Dives from the surface to 1000 m and back to the surface typically lasted about 5.5 hours. Vertically averaged currents were estimated from the difference between dead-reckoned and GPS-measured displacement during each dive as is typically done for underwater gliders [e.g., *Todd et al.*, 2009]. Pressure, temperature, salinity, and chlorophyll fluorescence were measured every 8 s during ascent, resulting in vertical resolution of about 0.8 m. The AD2CPs collected relative velocity measurements in 15 2-m bins below the gliders from 8-ping ensembles every 30 s during ascent. Following *Todd et al.* [2017], AD2CP measurements were quality controlled and combined with vertically averaged current estimates to produce vertical profiles of absolute horizontal velocity using an inverse method.

Cross-Gulf Stream transects from mission 15A065 (Fig. 2) illustrate how the glider observations capture the along-stream evolution of the Gulf Stream from its origins in the Florida Strait to downstream of its separation from the continental slope at Cape Hatteras, North Carolina. Following *Todd et al.* [2016], observations from each transect are shown as functions of cross-stream distance, which is determined by constructing a local streamwise coordinate system at the location of each glider dive with the downstream direction defined by the measured vertically averaged current; the origin of the cross-stream coordinate is taken to be the location at which the 15 °C isotherm is found at a depth of 200 m [*Fuglister and Voorhis*, 1965]. Expected cross-frontal temperature and salinity gradients are well-resolved by the high cross-stream resolution; the subsurface salinity maximum on the seaward side of the Gulf Stream [*Toole et al.*, 2011; *Qu et al.*, 2013; *Todd et al.*, 2016] can be traced from the Florida Strait to well downstream of Cape Hatteras (Figs. 2e–h). Downstream velocity structure from the glider-based AD2CP is consistent with previous direct velocity observations [e.g., *Halkin and Rossby*, 1985; *Rossby and Zhang*, 2001; *Shoosmith et al.*, 2005] and geostrophic estimates [e.g., *Todd et al.*, 2016] with a tilted Gulf Stream core, increasing speed and volume transport downstream, near surface velocities exceeding 2 m s^{-1} downstream of Cape Hatteras (Figs. 2i–l), and oppositely directed (equatorward) flow beneath the Gulf Stream near Cape Hatteras (Fig. 2k) as the Deep Western Boundary Current crosses under the Gulf Stream [*Pickart and Smethie*, 1993].

We combine observations from the ten glider missions by averaging observations from the 6246 distinct glider dives into $0.5° \times 0.5°$ boxes. Fig. 1d shows the number of dives in each box. Observations are reasonably dense along the path of the Gulf Stream from Miami to Cape Hatteras and between the New England continental shelf and Bermuda where trajectories from multiple missions overlapped (Fig. 1c), but are more sparse farther downstream (northeast) and in areas where only a single glider has sampled. Where we report average values of derived quantities in specific boxes in the text below, we report the standard deviation of the quantity of interest divided by the square root of the number of estimates as the standard error of the mean.

Averages of potential temperature at 200 m and vertically averaged currents in $0.5° \times 0.5°$ boxes show the expected O(1) m s^{-1} flow along the sharp temperature front of the Gulf Stream (Fig. 1e). Spatially and temporally sparse sampling results in transient Gulf Stream meanders and eddies appearing in these averages; for instance, a large, anticyclonic warm core ring discussed by *Cenedese et al.* [2013] appears near 38°N, 68°W, as does an anticyclone in the Sargasso Sea near 35°N, 72°W. However, in well sampled areas, details of the mean Gulf Stream structure, such as its eastward deflection at the Charleston Bump near 31.5°N [*Brooks and Bane*, 1978; *Gula et al.*, 2015], are apparent. We anticipate that inclusion of observations from ongoing Spray glider missions in the Gulf Stream will allow creation of a robust, high-resolution climatology of the Gulf Stream along the U.S. East Coast.

3. Results and Discussion

3.1. High-Frequency Internal Waves

The vertical motion of gliders was often strongly influenced by water motion. As an example, consider the time series of measured depth and its time derivative from dive 137 of mission 15A065 (Figs. 3a–b, blue), which took place near 31.7°N, 77.9°W over the northern Blake Plateau (Fig. 4, black circle). Throughout the dive, the glider's normally steady descent and ascent [cf. *Rudnick and Cole*, 2011, their Fig. 3] was alternately slowed and hastened by vertical water motion. Preceding and following dives (Figs. 3a–b, grey) were similarly affected, and gliders occasionally aborted dives (e.g., the missing data at a cross-stream distance of 20 km in Fig. 2b,f,j) when they were unable to descend against the ambient flow. The dive highlighted in Fig. 3 was within the Gulf Stream where estimated horizontal velocities from the glider's AD2CP exceeded 0.75 m s^{-1} from the surface to within a few meters of the acoustically estimated bottom depth of 639 m (Fig. 3d, red).

Following *Rudnick et al.* [2013], we use a model of glider flight to determine each glider's vertical speed through the water. This model-based estimate is subtracted from the actual vertical speed of the glider estimated from the rate of change of the glider's depth (inferred from measured pressure; e.g., Fig. 3b) to estimate the vertical velocity of the water throughout each glider dive (e.g., Fig. 3c) with an estimated error of 0.005 m s^{-1} [*Rudnick et al.*, 2013]. For dive 137 of mission 15A065, inferred vertical velocity exhibits oscillations with peak-to-trough ranges as large as 0.2 m s^{-1} and periods of 10–15 minutes; adjacent dives show similarly oscillating vertical velocities (Fig. 3c, grey). Vertical velocity oscillations at this period are consistent with internal waves at frequencies just below the local buoyancy frequency in the middle of the water column (i.e., away from weakly stratified surface and bottom layers; Fig. 3d, green). Assuming a simple sinusoidal dependence on time, the vertical velocity oscillations are consistent with waves having peak-to-trough vertical excursions of roughly 20–30 m. Large vertical velocities are found in the middle of the water column (e.g., Fig 3d), consistent with wave energy propagating upwards from generation sites at the seafloor upstream of the measurement site.

We use the standard deviation of inferred vertical velocity (e.g., Fig. 3c) as a metric of internal wave strength during each glider dive, and we average those standard deviations in $0.5° \times 0.5°$ boxes (Fig. 4a) to map out high-frequency internal wave activity. With average standard deviations of vertical velocity of 0.037 ± 0.003 m s^{-1}, the strongest internal waves, including the observations shown in Fig. 3, are found within the Gulf Stream near 31.75°N, 78.25°W as it passes over the rough topography associated with the Charleston Bump. Vertical velocities also tended to be large immediately before the point at which the Gulf Stream separates from the continental margin near Cape Hatteras where the upper slope is incised by many small canyons. The intensity of high-frequency internal waves falls off markedly away from the Blake Plateau.

We estimate the energy in observed internal waves using linear theory. For waves with vertical velocity w given by $w = w_0 \cos(kx + ly + mz - \omega t)$, with wave vector $\vec{K} = (k, l, m)$ and constant amplitude w_0, the frequency ω is related to the buoyancy frequency N by $\omega = \pm N \cos\vartheta$, where ϑ is the angle between the wave vector $\vec{K}$ and the horizontal plane [*Munk*, 1981; *Pedlosky*, 2003]. For $\omega \approx N$ as in our observations (e.g., Fig. 3), the wave vector is nearly horizontal and the vertical wavenumber m is approximately zero. It follows that the kinetic and potential energies averaged over a wave period are $\langle KE \rangle = \langle PE \rangle = \frac{1}{2}\rho_0 w_0^2$ and the total energy is simply $\langle E \rangle = \rho_0 w_0^2$, with ρ_0 a reference density [see *Pedlosky*, 2003, Lecture 8]. To estimate internal wave energy per unit horizontal area for each glider dive, we simply multiply the variance (i.e., the mean square deviations) of the vertical velocity time series (e.g., Fig. 3c) by the dive depth and $\rho_0 = 1026$ kg m^{-3}.

For the dive highlighted in Fig. 3, which sampled among the most energetic internal waves encountered, total energy is estimated at 1630 J m^{-2}. Average energy estimates in $0.5° \times 0.5°$ boxes (Fig. 4b) range as high as 855 ± 132 J m^{-2}. Highest internal wave energy is found near the Charleston Bump where internal wave amplitudes are largest (Fig. 4a) and modestly elevated internal wave energy is found farther downstream in the Gulf Stream; vertically integrated energy is lower along the upper continental slope due to the shallower depth. For comparison, estimates of full-depth-averaged energy density for the Hawaiian Ridge are 1–6 J m^{-3} at the 3000-m isobath [*Lee et al.*, 2006, their Fig. 4] and energy is concentrated in the thermocline with energy densities of 20–40 J m^{-3} at depths of 100–334 m [*Martin et al.*, 2006, their Fig. 5]; integrated vertically, these energy densities are equivalent to energy per unit horizontal area of approximately 3000–18000 J m^{-2}. The high-frequency waves generated as the Gulf Stream flows over the Blake Plateau and Charleston Bump may be 10–50% as energetic as those generated by the M_2 tide flowing over the much more prominent Hawaiian Ridge.

For a typical topographic height H of 100 m near the Charleston Bump (e.g., Fig. 1b and bathymetry in second row of Fig. 2), near-bottom velocities U of 0.5–1 m s^{-1} (e.g., Figs. 2j and 3d), and near-bottom buoyancy frequencies N of 2–7$\times 10^{-3}$ rad s^{-1} (periods of approximately 15–60 minutes; e.g., Fig 3d), the topographic Froude number for the Gulf Stream flowing over the Blake Plateau varies from 0.7–5. For this range of topographic Froude numbers, it is likely that the large-amplitude, high-frequency internal waves encountered by gliders are internal lee waves generated by sub-inertial flows with O(1) m s^{-1} near-bottom velocities over the varied bathymetry of the Blake Plateau. The frequency ω of such lee waves when following the flow is expected to be given by $\omega = \kappa U$, where κ is a characteristic wavenumber of the bathymetry. For the ranges of ω and U observed near the Charleston Bump, the corresponding topographic wavelength (and horizontal wavelength of resulting lee waves) would be O(1) km, suggesting that the observed lee waves result from flow over small scale bathymetric details. The estimated range of F_{topo} for Gulf Stream flow over the Blake Plateau spans the parameter range in which *Dossmann et al.* [2016] found breaking lee waves to contribute significantly to mixing as steady flows encounter topography.

3.2. Bottom Mixed Layers

Profiles of temperature, salinity, and density that reached the bottom often showed bottom mixed layers that were several tens of meters thick and occasionally exceeded 100 m in thickness over the Blake Plateau. Figs. 5a–d show an example from mission 157055 in which the bottom mixed layer thickness, Δz_{ml}, was 134 m as defined by a potential density difference of 0.01 kg m^{-3} from the deepest observation (which was measured 12 m above the bottom for this dive). For this example, horizontal current speed within the bottom mixed layer was approximately 0.7 m s^{-1} (Fig. 5d), indicating that the Gulf Stream reached to the bottom at this location near the Charleston Bump. Averages of observed bottom mixed layer thicknesses in $0.5^\circ \times 0.5^\circ$ boxes (Fig. 5e) suggest that enhanced mixing is prevalent near the Charleston Bump, where averaged mixed layer thickness is as large as 93 ± 10 m, and over deeper portions of the Blake Plateau. Modestly elevated mixed layer thicknesses are also found in the Florida Strait where *Seim et al.* [1999] and *Winkel et al.* [2002] found distinct homogenous bottom layers up to 60 m thick.

Formation of bottom mixed layers from an initial state of stable stratification requires kinetic energy from the local flow (i.e., the Gulf Stream) to be converted to potential energy in the bottom mixed layers. The change in potential energy due to formation of bottom mixed layers is $\Delta PE = \int_{-H}^{0} \Delta\sigma_\theta g z \, dz$, where the $\Delta\sigma_\theta$ is the difference between observed potential density profiles and corresponding 'pre-mixed' potential density profiles, g is gravity, and H is the bottom depth. We estimate a pre-mixed density gradient near the seafloor by combining all observed profiles of potential density anomalies relative to the densest measurements in each profile as a function of height above bottom. The average of such profiles is remarkably linear within 400 m of the seafloor, so we use a least squares fit to obtain a constant near-bottom density gradient of $\frac{\partial \sigma_\theta}{\partial z} = -0.002$ kg m^{-3} m^{-1}. Complete mixing of an initially linear density profile results in a change in potential energy of $\Delta PE = -\frac{g}{12}\frac{\partial \sigma_\theta}{\partial z}\Delta z_{\mathrm{ml}}^3$, where Δz_{ml} is the thickness of the resulting mixed layer and mass (i.e., the average density in the layer) is conserved (see Supporting Information). Since this change in potential energy is proportional to the cube of the mixed layer thickness, our estimates of the potential energy change associated with converting a uniformly-stratified water column to the observed bottom mixed layer features vary over more than an order of magnitude (Fig. 5f). Estimates of ΔPE exceed 4000 J m^{-2} for individual profiles (e.g., 4052 J m^{-2} for the the profile highlighted in Fig. 5) and average 2529 ± 739 J m^{-2} in the $0.5° \times 0.5°$ box near the Charleston Bump (Fig. 5f) that has the largest mean bottom mixed layer thickness (Fig. 5e). These estimates of energy required to form the observed mixed layers are conservative for two reasons: 1) inclusion of profiles with bottom mixed layers in our estimate of $\frac{\partial \sigma_\theta}{\partial z}$ lowers the estimate of the pre-mixed density gradient by approximately 20%; and 2) the estimate of ΔPE neglects the energy required for partial mixing above the bottom mixed layer, which must occur since sharp density gradients above the mixed layers (e.g., Fig. S1 in the Supporting Information) are generally not observed. For the example profile in Fig. 5c, a premixed density profile with $\frac{\partial \sigma_\theta}{\partial z} = -0.002$ kg m^{-3} m^{-1} would have to extend 37 m above the bottom mixed layer to conserve mass and be statically stable (Fig. 5c, red profile); the change in potential energy over the full-depth profile increases to 4451 J m^{-2}, a 10% increase over the estimate based only on the observed mixed layer thickness.

Consistent with the laboratory experiments of *Dossmann et al.* [2016], we attribute the formation of the thick bottom mixed layers reported here to turbulent mixing in the lee of topographic features encountered by the Gulf Stream. *Nash and Moum* [2001] detailed similar elevated mixing in the lee of a small bank on the Oregon continental shelf. We note that our estimates of the potential energy change associated with converting a uniformly-stratified water column to the observed bottom mixed layer features (Fig. 5c) are several times larger than the total energy in the high-frequency internal waves (Fig. 4b), in line with the conclusion of *Dossmann et al.* [2016] that mid-water column mixing due to lee wave radiation is limited to intermediate topographic Froude numbers ($F_{\text{topo}} \sim 1 - 2$). With topographic Froude numbers less than unity over portions of Blake Plateau, the flow over the larger topography (e.g., the Charleston Bump) is likely to form stratified hydraulic jumps and associated static instabilities downstream of topography as well as shear instabilities. Both of these turbulent processes lead to energy dissipation and mixing [*Klymak and Gregg*, 2004; *Inall et al.*, 2005] and are likely mechanisms contributing to formations of the thickest bottom mixed layers observed by gliders over Blake Plateau.

4. Summary

Spray gliders provide high-resolution transects across the Gulf Stream along the U.S. East Coast. Despite their slow speed, the gliders are able to navigate back and forth across the Gulf Stream as they are advected downstream by it (e.g., Fig. 1c). Sustained glider surveys in the Gulf Stream offer the opportunity fill a significant gap in subsurface monitoring of the Gulf Stream between the Florida Strait [*Baringer and Larsen*, 2001; *Shoosmith et al.*, 2005] and the M/V *Oleander* line that samples between New Jersey and Bermuda [e.g., *Flagg et al.*, 2006] and serve as a model for autonomous sampling in western boundary currents to complement the basin-scale coverage of the Argo program [e.g., *Riser et al.*, 2016]. Addition of observations from ongoing Spray glider surveys will eventually allow construction of a robust, high-resolution climatology of the Gulf Stream along the U.S. East Coast.

Observations from ten Spray glider missions in the Gulf Stream highlight two mechanisms by which energy is extracted from the gyre-scale flow. As the Gulf Stream flows over the varied topography of the Blake Plateau, internal lee waves with frequencies near the buoyancy frequency are generated (e.g., Fig. 3) and bottom mixed layers with thicknesses exceeding 100 m are formed (e.g., Fig. 5a–d). The spatial coverage of the glider surveys demonstrates that both mechanisms are most prevalent in the vicinity of the Charleston Bump, a prominent topographic feature encountered by the Gulf Stream near 31.5°N (Figs. 4 and 5e–f), and we are able to estimate the energy in both the high-frequency waves and the bottom mixed layers. Much of the spatial variability in internal waves (Figs. 4) and bottom mixed layers (Figs. 5e–f) may be attributed to temporal variability in Gulf Stream strength, position, and orientation relative to the bathymetry [e.g., *Bane and Dewar*, 1988]. The glider observations lack the vertical and temporal resolution to directly measure turbulent mixing associated with these features, and the gliders are unable to hold station in the Gulf Stream to observe temporal evolution of the internal wave field and bottom mixed layers; a process study focused on internal wave generation and near-bottom mixing with appropriate instrumentation is warranted. These processes that remove energy from the Gulf Stream, along with the elevated internal wave activity reported by *Clément et al.* [2016] as eddies impinge upon the western boundary near 26.5°N, highlight the importance of western boundaries as locations where the energy input to the oceans at large scales is transferred to smaller scales and ultimately dissipated.

Acknowledgments. The author thanks Dan Rudnick and Breck Owens for encouraging him to conduct new glider surveys in the Gulf Stream and for supporting the effort. Discussions with John Toole significantly improved the analysis. Larry George, Patrick Deane, and Ben Hodges at WHOI and Jeff Sherman, Kyle Grindley, Ben Reineman, and Evan Randall-Goodwin of the Instrument Development Group at the Scripps Institution of Oceanography were key to the success of the Spray glider operations. The Physical Oceanography Division at NOAA's Atlantic Oceanographic and Meteorological Laboratory (AOML) provided laboratory space for glider preparation, and North Carolina State University's Center for Marine Sciences and Technology (CMAST) provided laboratory space following recovery of one of the gliders. Spray glider observations in the Gulf Stream are available from http://spraydata.ucsd.edu and should be cited using the following DOI: 10.21238/S8SPRAY2675. We gratefully acknowledge funding from the National Science Foundation (OCE-0220769,OCE-1633911), the Office of Naval Research (N000141713040), NOAA's Climate Observation Division (NA14OAR4320158), Eastman Chemical Company, WHOI's Oceans and Climate Change Institute, and the W. Van Alan Clark, Jr. Chair for Excellence in Oceanography at WHOI (awarded to Breck Owens).

References

Alford, M. H., J. A. MacKinnon, J. D. Nash, H. Simmons, A. Pickering, J. M. Klymak, R. Pinkel, O. Sun, L. Rainville, R. Musgrave, T. Beitzel, K.-H. Fu, and C.-W. Lu (2011), Energy flux and dissipation in Luzon Strait: Two tales of two ridges, *J. Phys. Oceanogr.*, *41*, 2211–2222, doi:10.1175/JPO-D-11-073.1.

Bane, J. M., Jr., and W. K. Dewar (1988), Gulf Stream bimodality and variability downstream of the Charleston Bump, *J. Geophys. Res.*, *93*(C6), 6695–6710, doi:10.1029/JC093iC06p06695.

Baringer, M. O., and J. C. Larsen (2001), Sixteen years of Florida Current transport at 27°N, *Geophys. Res. Lett.*, *28*(16), 3179–3182, doi:10.1029/2001GL013246.

Bell, T., Jr. (1975), Topographically generated internal waves in the open ocean, *J. Geophys. Res.*, *80*(3), 320–327, doi:10.1029/JC080i003p00320.

Brooks, D. A., and J. M. Bane (1978), Gulf Stream deflection by a bottom feature off Charleston, South Carolina, *Science*, *201*(4362), 1225–1226, doi:10.1126/science.201.4362.1225.

Cenedese, C., R. E. Todd, G. G. Gawarkiewicz, W. B. Owens, and A. Y. Shcherbina (2013), Offshore transport of shelf waters through interaction of vortices with a shelf-break current, *J. Phys. Oceanogr.*, *43*(5), 905–919, doi:10.1175/JPO-D-12-0150.1.

Clément, L., E. Frajka-Williams, K. L. Sheen, J. A. Brearley, and A. C. Naveira Garabato (2016), Generation of internal waves by eddies impinging on the western boundary of the North Atlantic, *J. Phys. Oceanogr.*, *46*, 1067–1079, doi:10.1175/JPO-D-14-0241.1.

Cole, S. T., D. L. Rudnick, B. A. Hodges, and J. P. Martin (2009), Observations of Tidal Internal Wave Beams at Kauai Channel, Hawaii, *J. Phys. Oceanogr.*, *39*, 421–436, doi: 10.1175/2008JPO3937.1.

Dossmann, Y., M. G. Rosevar, R. W. Griffiths, A. M. Hogg, G. O. Hughes, and M. Copeland (2016), Experiments with mixing in stratified flow over a topographic ridge, *J. Geophys. Res.*, *121*, 6961–6977, doi:10.1002/2016JC011990.

Ferron, B., H. Mercier, K. Speer, A. Gargett, and K. L. Polzin (1998), Mixing in the Romanche Fracture Zone, *J. Phys. Oceanogr.*, *28*, 1929–1945, doi:10.1175/1520-0485(1998)028¡1929:MITRFZ¿2.0.CO;2.

Flagg, C. N., M. Dunn, D.-P. Wang, H. T. Rossby, and R. L. Benway (2006), A study of the currents of the outer shelf and upper slope from a decade of shipboard ADCP observations in the Middle Atlantic Bight, *J. Geophys. Res.*, *111*, C06003, doi: 10.1029/2005JC003116.

Fuglister, F. C., and A. D. Voorhis (1965), A new method of tracking the Gulf Stream, *Limnol. Oceanogr.*, *10*(Supplement: Alfred C. Redfield 75th Anniversary Volume), 115–124, doi:10.4319/lo.1965.10.suppl2.r115.

Gill, A. E. (1982), *Atmosphere-Ocean Dynamics*, *International Geophysics Series*, vol. 30, Academic Press, San Diego, Calif.

Gula, J., M. J. Molemaker, and J. C. McWilliams (2015), Gulf Stream dynamics along the southeastern U.S. seaboard, *J. Phys. Oceanogr.*, *45*, 690–715, doi:10.1175/JPO-D-14-0154.1.

Halkin, D. T., and H. T. Rossby (1985), The structure and transport of the Gulf Stream at 73°W, *J. Phys. Oceanogr.*, *15*, 1439–1452, doi:10.1175/1520-0485(1985)015¡1439:TSATOT¿2.0.CO;2.

Inall, M., T. Rippeth, C. Griffiths, and P. Wiles (2005), Evolution and distribution of TKE production and dissipation within stratified flow over topography, *Geophys. Res. Lett.*, *32*, doi:10.1029/2004GL022289.

Klymak, J. M., and M. C. Gregg (2004), Tidally generated turbulence over the Knight Inlet sill, *J. Phys. Oceanogr.*, *34*, 1135–1151, doi:10.1175/1520-0485(2004)034¡1135:TGTOTK¿2.0.CO;2.

Klymak, J. M., J. N. Moum, J. D. Nash, E. Kunze, J. B. Girton, G. S. Carter, C. M. Lee, T. B. Sanford, and M. C. Gregg (2006), An estimate of tidal energy lost to turbulence at the Hawaiian Ridge, *J. Phys. Oceanogr.*, *36*, 1148–1164, doi:10.1175/JPO2885.1.

Klymak, J. M., S. M. Legg, and R. Pinkel (2010), High-mode stationary waves in stratified flow over large obstacles, *J. Fluid Mech.*, *644*, 321–336, doi:10.1017/S0022112009992503.

Lee, C. M., E. Kunze, T. B. Sanford, J. D. Nash, M. A. Merrifield, and P. E. Holloway (2006), Internal tides and turbulence along the 3000-m isobath of the Hawaiian Ridge, *J. Phys. Oceanogr.*, *36*, 1165–1183, doi:10.1175/JPO2886.1.

Martin, J. P., and D. L. Rudnick (2007), Inferences and observations of turbulent dissipation and mixing in the upper ocean at the Hawaiian Ridge, *J. Phys. Oceanogr.*, *37*(3), 476–494.

Martin, J. P., D. L. Rudnick, and R. Pinkel (2006), Spatially Broad Observations of Internal Waves in the Upper Ocean at the Hawaiian Ridge, *J. Phys. Oceanogr.*, *36*, 1085–1103.

Miles, J. W., and H. E. Huppert (1968), Lee waves in stratified flow. Part 2. Semi-circular obstacle, *J. Fluid Mech.*, *33*(4), 803–814, doi:10.1017/S0022112068001680.

Munk, W. (1981), Internal Waves and Small-Scale Processes, in *Evolution of Physical Oceanography–Scientific Surveys in Honor of Henry Stommel*, edited by B. Warren and C. Wunsch, chap. 9, pp. 264–291, Mass. Inst. of Technol., Boston.

Munk, W., and C. Wunsch (1998), Abyssal recipes II: energetics of tidal and wind mixing, *Deep-Sea Res. I*, *45*, 1977–2010.

Munk, W. H. (1966), Abyssal recipes, *Deep-Sea Res.*, *13*, 707–730.

Nash, J. D., and J. N. Moum (2001), Internal hydraulic flows on the continental shelf: High drag states over a small bank, *J. Geophys. Res.*, *106*(C3), 4593–4611.

Nikurashin, M., and R. Ferrari (2011), Global energy conversion rate from geostrophic flows into internal lee waves in the deep ocean, *Geophys. Res. Lett.*, *38*, L08,610, doi: 10.1029/2011GL046576.

Pedlosky, J. (2003), *Waves in the Ocean and Atmosphere*, Springer-Verlag, Berlin.

Pickart, R. S., and W. M. Smethie (1993), How does the Deep Western Boundary Current cross the Gulf Stream?, *J. Phys. Oceanogr.*, *23*, 2602–2616.

Polzin, K. L., K. G. Speer, J. M. Toole, and R. W. Schmitt (1996), Intense mixing of Antarctic Bottom Water in the equatorial Atlantic Ocean, *Nature*, *380*, 54–57, doi: 10.1038/380054a0.

Polzin, K. L., J. M. Toole, J. R. Ledwell, and R. W. Schmitt (1997), Spatial Variability of Turbulent Mixing in the Abyssal Ocean, *Science*, *276*(5309), 93–96, doi:

10.1126/science.276.5309.93.

Pratt, R. M. (1963), Bottom currents on the Blake Plateau, *Deep-Sea Res.*, *10*, 245–249, doi:10.1016/0011-7471(63)90360-7.

Pratt, R. M., and B. C. Heezen (1964), Topography of the Blake Plateau, *Deep-Sea Res.*, *11*, 721–728, doi:10.1016/0011-7471(64)90945-3.

Qu, T., S. Gao, and I. Fukumori (2013), Formation of salinity maximum water and its contribution to the overturning circulation in the North Atlantic as revealed by a global general circulation model, *J. Geophys. Res.*, *118*, 1982–1994, doi:10.1002/jgrc.20152.

Riser, S. C., H. J. Freeland, D. Roemmich, S. Wijffels, A. Troisi, M. Belbéoch, D. Gilbert, J. Xu, S. Pouliquen, A. Thresher, P.-Y. L. Traon, G. Maze, B. Klein, M. Ravichandran, F. Grant, P.-M. Poulain, T. Suga, B. Lim, A. Sterl, P. Sutton, K.-A. Mork, P. J. Vélez-Belchi, I. Ansorge, B. King, J. Turton, M. Baringer, and S. R. Jayne (2016), Fifteen years of ocean observations with the global Argo array, *Nat. Climate Change*, *6*, 145–153, doi:10.1038/NCLIMATE2872.

Rossby, T., and H.-M. Zhang (2001), The near-surface velocity and potential vorticity structure of the Gulf Stream, *J. Mar. Res.*, *59*, 949–975.

Rudnick, D. L., and S. T. Cole (2011), On sampling the ocean using underwater gliders, *J. Geophys. Res.*, *116*, C08010, doi:10.1029/2010JC006849.

Rudnick, D. L., T. J. Boyd, R. E. Brainard, G. S. Carter, G. D. Egbert, M. C. Gregg, P. E. Holloway, J. M. Klymak, E. Kunze, C. M. Lee, M. D. Levine, D. S. Luther, J. P. Martin, M. A. Merrifield, J. N. Moum, J. D. Nash, R. Pinkel, L. Rainville, and T. B. Sanford (2003), From tides to mixing along the Hawaiian ridge, *Science*, *301*(5631), 355–357, doi:10.1126/science.1085837.

Rudnick, D. L., T. M. S. Johnston, and J. T. Sherman (2013), High-frequency internal waves near the Luzon Strait observed by underwater gliders, *J. Geophys. Res.*, *118*, 1–11, doi:10.1002/jgrc.20083.

Seim, H. E., D. P. Winkel, G. G. Gawarkiewicz, and M. C. Gregg (1999), A benthic front in the Straits of Florida and its relationship to the structure of the Florida Current, *J. Phys. Oceanogr.*, *29*, 3125–3132, doi:10.1175/1520-0485(1999)029¡3125:ABFITS¿2.0.CO;2.

Sherman, J., R. E. Davis, W. B. Owens, and J. Valdes (2001), The autonomous underwater glider "Spray", *IEEE J. Oceanic Eng.*, *26*(4), 437–446, doi:10.1109/48.972076.

Shoosmith, D. R., M. O. Baringer, and W. E. Johns (2005), A continuous record of Florida Current temperature transport at 27°N, *Geophys. Res. Lett.*, *32*, L23,603, doi:10.1029/2005GL024075.

St. Laurent, L., A. C. Naveira Garabato, J. R. Ledwell, A. M. Thurnherr, J. M. Toole, and A. J. Watson (2012), Turbulence and diapycnal mixing in Drake Passage, *J. Phys. Oceanogr.*, *42*, 2143–2152, doi:10.1175/JPO-D-12-027.1.

Todd, R. E., D. L. Rudnick, and R. E. Davis (2009), Monitoring the greater San Pedro Bay region using autonomous underwater gliders during fall of 2006, *J. Geophys. Res.*, *114*, C06001, doi:10.1029/2008JC005086.

Todd, R. E., W. B. Owens, and D. L. Rudnick (2016), Potential vorticity structure in the North Atlantic western boundary current from underwater glider observations, *J. Phys. Oceanogr.*, *46*(1), 327–348, doi:10.1175/JPO-D-15-0112.1.

Todd, R. E., D. L. Rudnick, J. T. Sherman, W. B. Owens, and L. George (2017), Absolute velocity estimates from autonomous underwater gliders equipped with Doppler current profilers, *J. Atmos. Oceanic Technol.*, *34*(2), 309–333, doi:10.1175/JTECH-D-16-0156.1.

Toole, J. M., R. G. Curry, T. M. Joyce, M. McCartney, and B. Peña Molino (2011), Transport of the North Atlantic Deep Western Boundary Current about 39°N, 70°W: 2004–2008, *Deep-Sea Res. II*, *58*, 1768–1780, doi:10.1016/j.dsr2.2010.10.058.

Winkel, D. P., M. C. Gregg, and T. B. Sanford (2002), Patterns of shear and turbulence across the Florida Current, *J. Phys. Oceanogr.*, *32*, 3269–3285, doi:10.1175/1520-0485(2002)032¡3269:POSATA¿2.0.CO;2.

Wunsch, C. (1998), The work done by the wind on the oceanic general circulation, *J. Phys. Oceanogr.*, *28*, 2332–2340, doi:10.1175/1520-0485(1998)028¡2332:TWDBTW¿2.0.CO;2.

Wyrtki, K., L. Magaarda, and J. Hager (1976), Eddy energy in the oceans, *J. Geophys. Res.*, *81*(15), 2641–2646, doi:10.1029/JC081i015p02641.

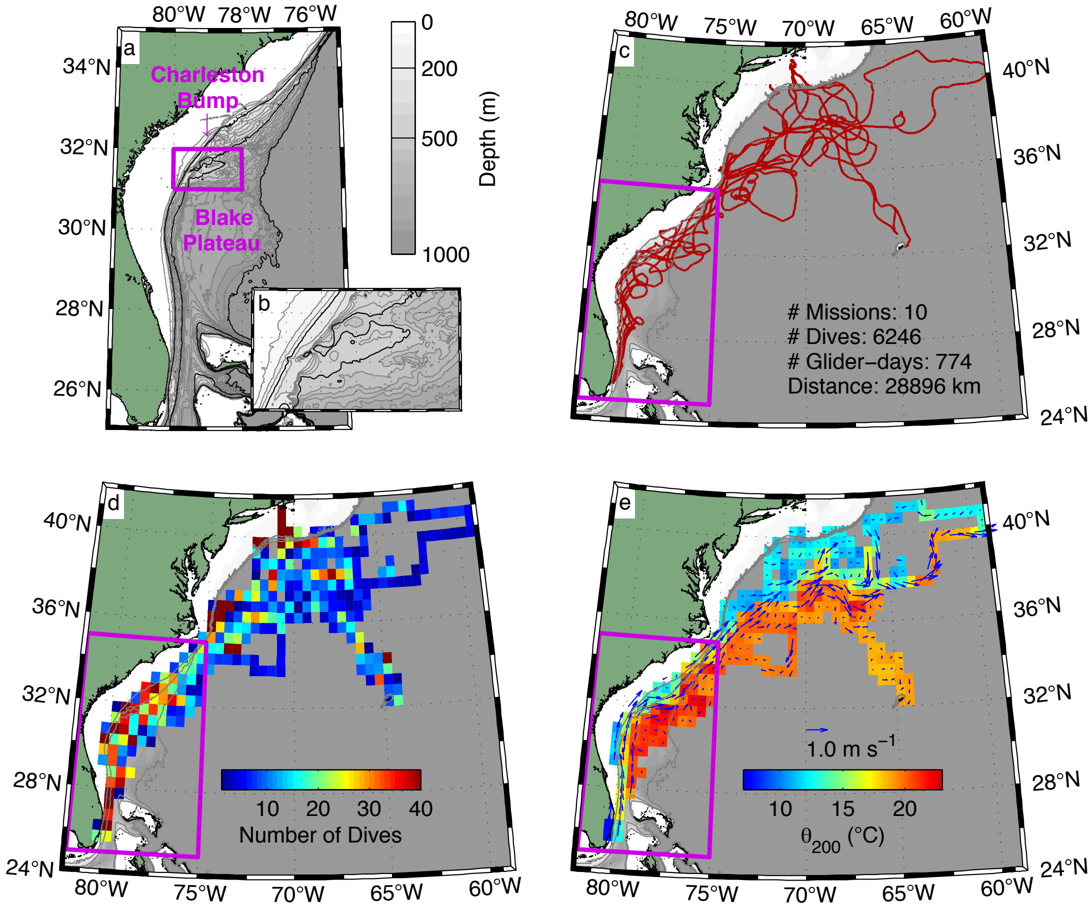

Figure 1. (a) Bathymetry of the outer continental shelf from the Florida Strait to near Cape Hatteras including the Blake Plateau and Charleston Bump (magenta box in c–e) with grey isobaths every 50 m and the 200-, 500-, and 1000-m isobaths drawn black. (b) Detail of the bathymetry of the Charleston Bump, corresponding to the magenta box in (a). The color scale for shaded bathymetry is common for all panels. (c) Trajectories of completed Spray glider missions in and near the Gulf Stream from 2004 through early 2017 with summary statistics. (d) Number of glider dives within 0.5° × 0.5° boxes. (e) Grand averages of potential temperature at 200 m (θ_{200}) and vertically averaged currents in 0.5° × 0.5° boxes. A scale vector is shown near 30°N, 70°W. In (c–e), the 200-, 500-, and 1000-m isobaths are drawn grey.

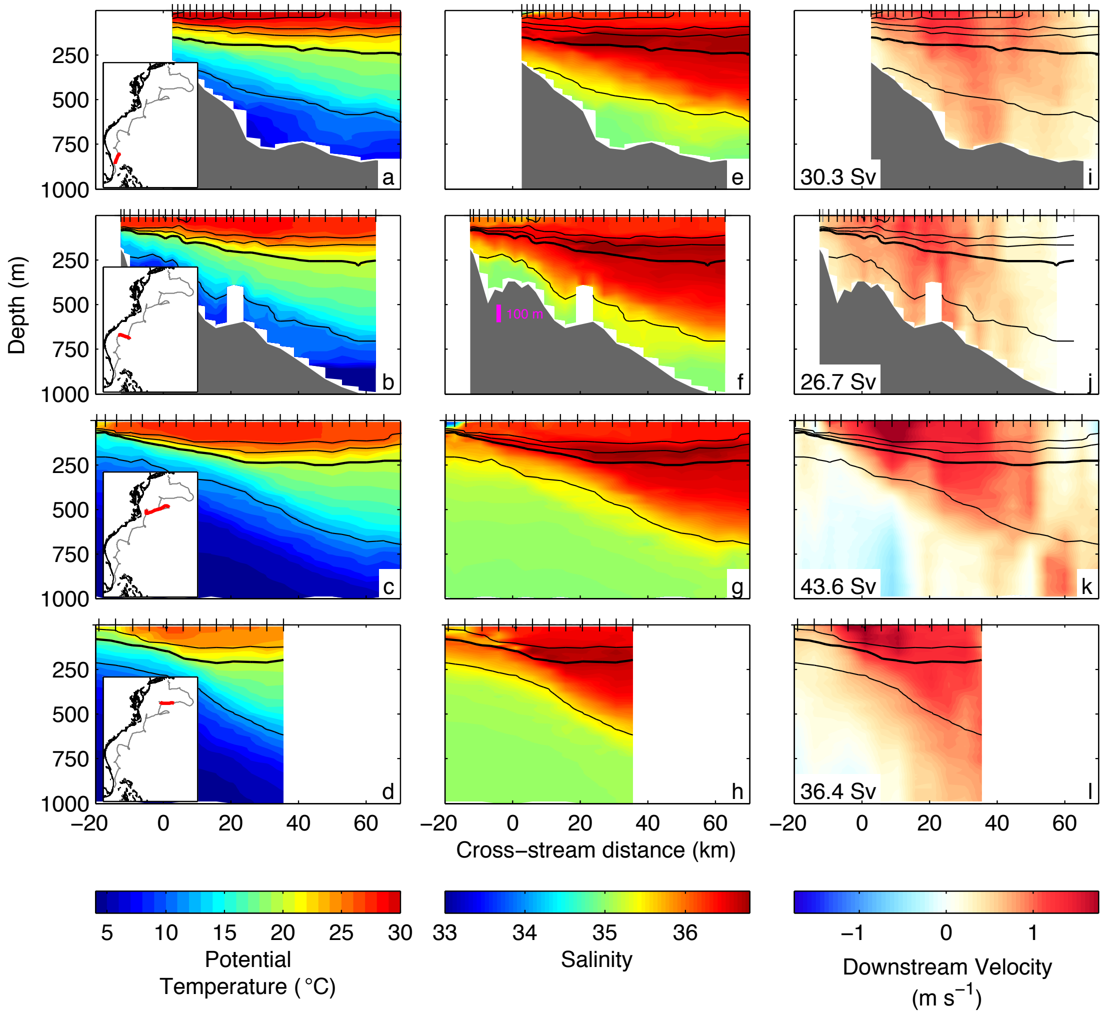

Figure 2. Example cross-Gulf Stream transects of (a–d) potential temperature, (e–h) salinity, and (i–l) downstream velocity from Spray glider mission 15A065. Transects are progressively farther downstream from top to bottom with inset maps in the left column showing the glider's track in grey with the corresponding transect highlighted in red. Black contours indicate isopycnals with a contour interval of 1.0 kg m^{-3} and the 26.0 kg m^{-3} isopycnal bold. Alongstream volume transports for each transect are given in (i–l), where the integration includes only positive (downstream) velocity estimates to isolate Gulf Stream flow. Grey shading indicates the location of the seafloor using the AD2CP's altimeter functionality and a 100-m vertical scale in included in (f). Tick marks on the upper axes of each panel indicate the locations of individual profiles.

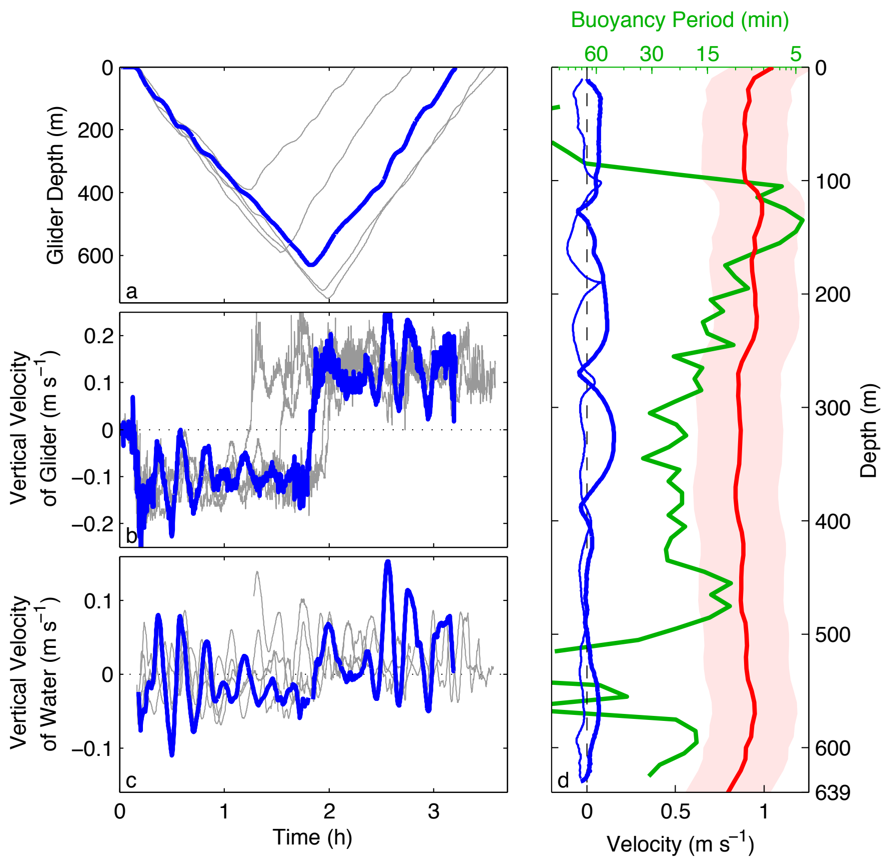

Figure 3. Example observations of internal waves from mission 15A065. Timeseries of (a) glider depth, (b) raw vertical velocity of the glider ($\frac{dz}{dt}$), and (c) inferred vertical velocity of the water, respectively. Dive 137 is shown blue with the preceding and following two dives shown grey. (d) Vertical profiles from dive 137 of squared Brunt-Väisälä frequency (N^2) with oscillation period denoted (green), vertical velocity during the ascending (heavy blue) and descending (thin blue) portions of the dive (blue, from panel c), and horizontal current speed (red) with shading denoting the root-mean-square error in velocity at the bottom of profiles from *Todd et al.* [2017]. The location of dive 137 is shown in Fig. 4.

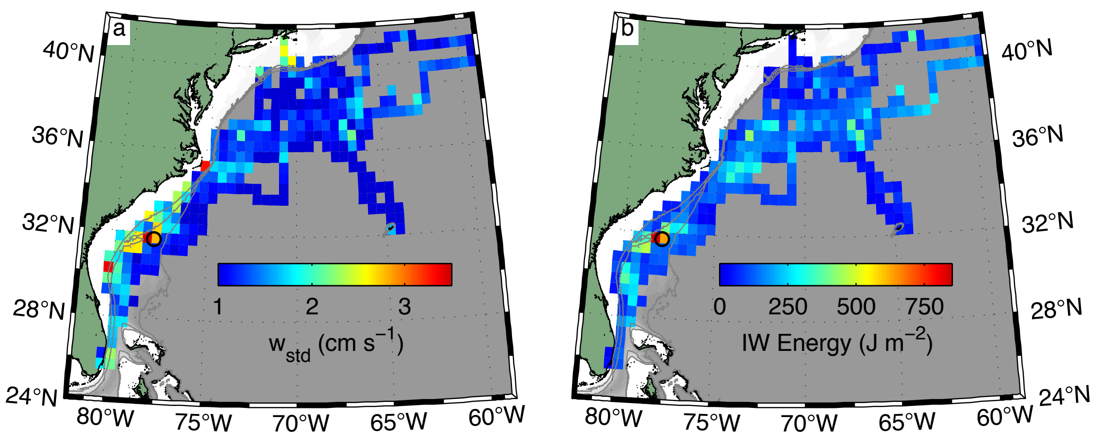

Figure 4. Amplitude and total energy of high-frequency internal waves. (a) Standard deviations of vertical velocities from individual glider dives averaged in $0.5^\circ \times 0.5^\circ$ boxes. (b) Vertically integrated internal wave energy averaged in the same boxes. Bathymetry is as in Fig. 1 with the 200-, 500-, and 1000-m isobaths drawn grey. The black circles are centered on the location of the dive focused on in Fig. 3.

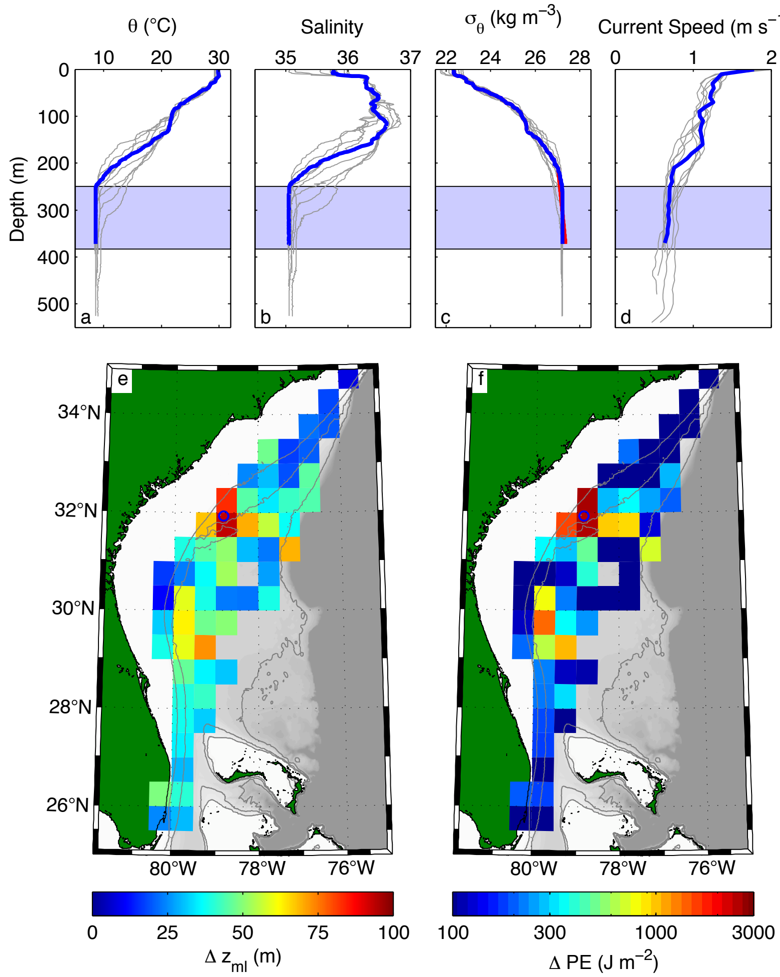

Figure 5. Bottom mixed layers over the Blake Plateau and Charleston Bump. Example profiles of (a) potential temperature θ, (b) salinity, (c) potential density σ_θ, and (d) horizontal current speed from mission 157055 in the vicinity of 32°N, 79°W. Profiles from dive 182 are shown blue with the preceding and following four dives shown grey. Blue shading denotes the bottom mixed layer for dive 182. The red density profile in (c) is an estimated 'pre-mixed' profile for dive 182 with a density gradient of $\frac{d\sigma_\theta}{dz} = -0.002$ kg m^{-3} m^{-1} below 217 m. (e) Observed bottom mixed layer thicknesses and (f) estimated changes in potential energy ΔPE required to form the mixed layers averaged in 0.5° × 0.5° boxes. Only the region southwest of Cape Hatteras where gliders dove near the seafloor (inset region in Fig. 1) is shown. The blue circles in (e) and (f) show the location of the profiles in (a–d).